Preprint Cambridge Centre for Computational Chemical Engineering ISSN 1473 – 4273

# A multidimensional population balance model to describe the aerosol synthesis of silica nanoparticles.

Shraddha Shekar [1], Alastair J. Smith [1], William Menz [1], Markus Sander [1], Markus Kraft [1]

released: 16 May 2011

[1] Department of Chemical Engineering
and Biotechnology
University of Cambridge
New Museums Site
Pembroke Street
Cambridge, CB2 3RA
UK
E-mail: mk306@cam.ac.uk

Preprint No. 103


*Keywords:* silica nanoparticle, aerosol synthesis, kinetic model, particle model, optimisation

**Edited by**
Computational Modelling Group
Department of Chemical Engineering and Biotechnology
University of Cambridge
New Museums Site
Pembroke Street
Cambridge CB2 3RA
United Kingdom

**Fax:** + 44 (0)1223 334796
**E-Mail:** c4e@cam.ac.uk
**World Wide Web:** http://como.cheng.cam.ac.uk/

**Abstract**

The aim of this work is to present a new detailed multivariate population balance model to describe the aerosol synthesis of silica nanoparticles from tetraethoxysilane (TEOS). The new model includes a chemical representation of the silica particles to facilitate a detailed chemical description of particle processes. Silica nanoparticles are formed by the interaction of silicic acid monomers ($Si(OH)_4$) in the gas-phase as reported in a previous study. A multidimensional population balance model is developed where each particle is described by its constituent primary particles and the connectivity between these primaries. Each primary, in turn, has internal variables that describe its chemical composition, *i.e.* , the number of Si, free O and OH units. Different particle processes, such as inception, surface reaction, coagulation, sintering, and intra-particle reactions, are formulated from first-principles that alter the particle ensemble and are two-way coupled to the gas-phase. The free parameters in the model are estimated by fitting the model response to experimental values of collision and primary particle diameters using low discrepancy Sobol sequences followed by the simultaneous perturbation stochastic approximation algorithm. The simulation results are finally presented at different process conditions. A strong dependence of particle properties on process temperature and inlet concentration is observed. The desirable operating conditions for different industrial applications are also highlighted. This work illustrates the significance of adopting a multidimensional approach to understand, and hence control, complex nanoparticle synthesis processes.

# Contents

# 1 Introduction

The flame synthesis and characterisation of silica nanoparticles (SiNP) on an industrial scale has received considerable attention in the last decade due to their large range of practical applications. The most popular route of industrial synthesis of inorganic nanoparticles is via flame spray pyrolysis of a wide array of precursors [13, 34]. Tetraethoxysilane (TEOS) as a halide-free and inexpensive starting material is widely used as a precursor for the manufacture of SiNP. Silica nanoparticles find applications in ceramics, catalysis, chromatography, as a filler and binding material to improve material properties [10] and as functional materials to form nanocomposites. Recent discoveries have reported the use of SiNP for bio-imaging and drug delivery [29]. Such sensitive applications require particles of highly specific size, morphology and surface characteristics. In order to control the particle properties, it is essential to understand the detailed mechanism of formation and growth of these nanoparticles.

Various studies have been conducted to investigate the formation of silica nanoparticles from TEOS in the vapour phase using different methods. Smolík and Moravec [30] examined the production of silica particles by thermal decomposition of TEOS vapour in the presence of oxygen using Chemical Vapour Deposition (CVD) techniques. Jang [11] synthesised silica nanoparticles from TEOS vapour in a laminar diffusion flame reactor and characterised the particles at different operating conditions. The formation and sintering of silica particles in a heated pipe was studied by Seto et al. [26]. The effect of temperature on the particle structure and size distribution was examined by first generating the particles at 900 °C and then heating the particles to different final temperatures. Due to the lack of a detailed kinetic model in previous studies, the flame synthesis of silica nanoparticles from TEOS was assumed to proceed via the sticking of gaseous $SiO_2$ monomers. Recent kinetic studies on the flame synthesis of silica nanoparticles from tetraethoxysilane (TEOS) suggest the formation of nanoparticles via the interaction of silicic acid ($Si(OH)_4$) monomers [9, 21, 27]. This work is developed under the framework that the formation of silica nanoparticles proceeds through the dehydration of silicic acid monomers.

Previous population balance models in the field of nanoparticle synthesis have focussed on tracking a single property in the particle ensemble, typically particle diameter or size. A one-dimensional population balance model was first used to simulate particle dynamics of flame-synthesised pyrogenic silica by Ulrich [37]. The one-dimensional approach was extended to two-dimensions by Xiong et al. [39] who studied the evolution of particle size and shape by coagulation and sintering using a population balance equation which was solved by sectional methods. Tsantilis et al. [36] used a similar approach to model the flame synthesis of titania nanoparticles. The growth of non-spherical silica particles in a counterflow diffusion flame was analysed by Lee et al. [16] where in addition to coagulation, they consider the effect of chemical reactions and coalescence.

In this work, we use a stochastic population balance approach to study the formation of silica nanoparticles formed from silicic acid monomers. The use of stochastic methods to solve population balance equations provides an advantage over sectional methods as they are suitable for problems of high dimension. A stochastic particle algorithm to solve the Smoluchowski coagulation equation has been developed by Eibeck and Wagner [5] and improved upon by Goodson and Kraft [7] and Patterson and Kraft [19]. Morgan et al. [18]

have extended this algorithm to include particle inception, surface growth and sintering. Celnik et al. [3, 4] incorporated the effects of gas-phase reactions into the stochastic population balance model by using an operator splitting technique, and West et al. [38] used such a coupled model to study the synthesis of titania particles. Previous works in the field of population balance modelling of nanoparticles have been restricted to defining the particle ensemble only in terms of its shape and/or size. The motivation behind the current work is to expand the scope of the previous models by describing the particle formation mechanism in an unprecedented level of detail by tracking the evolution of the individual chemical units in each particle in the ensemble. By including a compositional representation of the nanoparticles, various particle properties can be calculated more accurately and a more refined chemical description of different particle processes can be furnished.

The aims of this work are threefold: (i) To develop a multidimensional population balance model that describes the evolution of the chemical composition of silica nanoparticles synthesised by flame pyrolysis of TEOS; (ii) To estimate the free-parameters of the model by fitting it to experimental data; (iii) To report the model response at different process conditions.

The paper is structured as follows: A description of the stochastic particle model is given in §2. The different particle processes such as surface reaction, coagulation, sintering and intra-particle reactions that transform the particles are described in §2.1. The rates of each of these processes are described in §2.2. The stoichiometric ratio of Si:O is constrained to 1:2 and is applied in §2.3 to deduce the rate of the intra-particle process. The estimation of free parameters in the model is described in §3. This section also presents the comparision of model predictions to experimental data along with the computer generated TEM images. Finally, simulation results are presented in §4, where industrially relevant particle properties are reported at different process conditions. The paper concludes with a discussion of the advantages of the new detailed model and its limitations, along with potential steps for future research.

# 2 Silica particle model

The population balance model used in the current work enables us to track the properties of silica nanoparticles in an unprecedented level of detail. Various particle processes that alter the particles are also included in the model. Tracking the chemical composition of the particles allows us not only to describe the particle properties more accurately, but also provides better coupling of the gas-phase to the particle-phase, because each of the particle processes altering the gas-phase composition are accounted for. In this section, the representation of the particle and the different particle processes are outlined.

From a previous study [27], we conclude that the main product of TEOS decomposition is silicic acid ($Si(OH)_4$). The main particle formation pathway is given in **Fig. 1**.

It is proposed that the particle is formed due to the inception of $Si(OH)_4$ in gas-phase. The dehydration of two silicic acid monomers leads to the inception of the first particles. The particles then grow by coagulation, surface reaction, intra-particle reactions and sintering as described in the following sections. The detailed mathematical description and

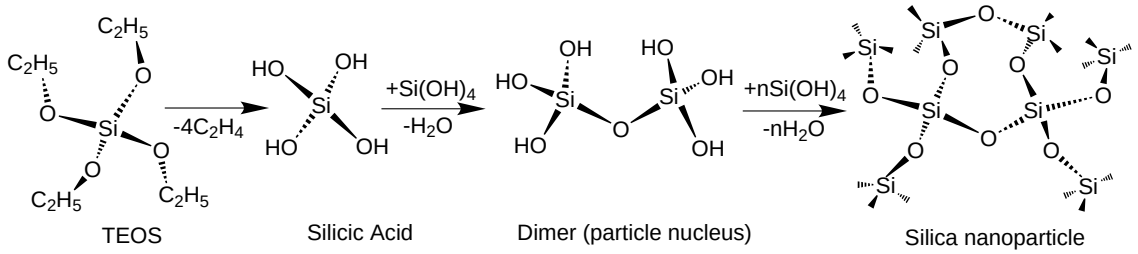


***Figure 1:*** *The pathway for silica nanoparticle formation.*

numerical properties of this model have been presented elsewhere [28]. Each particle is represented in terms of its primary particles and the connectivity between these primaries. The connectivity is represented as a matrix containing the common surface of a given primary with all of the other primaries in a particle. If the primaries are non-neighbouring, then their common surface is zero; if the primaries are at point contact, there common surface is the sum of the individual surfaces and if the primaries are completely sintered then there common surface is replace by the surface of a sphere with the same volume as that of the individual primaries. Each primary in turn is described by its chemical composition *i.e.* , the number of Si, O and OH units it contains. The description of a single particle in the system is schematically represented in **Fig. 2**. All the derived properties of the particle (mass, surface area, volume *etc.* ) are then described in terms of the internal variables defined above.

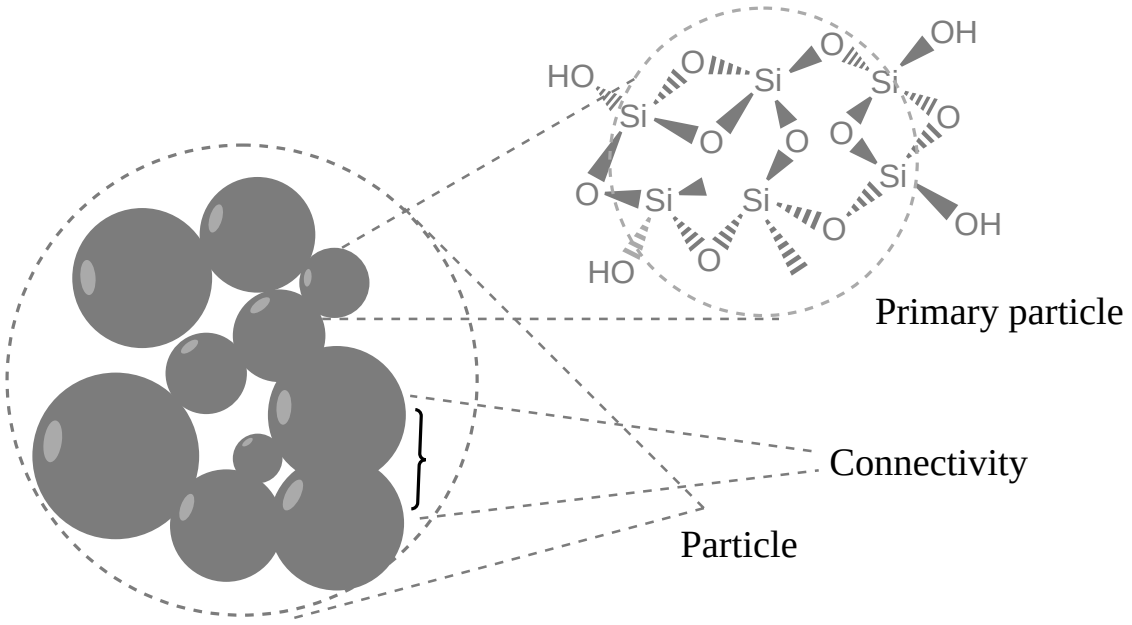


***Figure 2:*** *Representation of the internal variables used to describe a single particle in the particle ensemble.*

## 2.1 Particle processes

During the course of its lifetime, a particle in the system evolves due to various processes, namely: inception, surface reaction, coagulation, sintering and intra-particle reaction. These processes along with their rates and transformations are described below:

- **Inception:** Two molecules in gas phase collide to form a particle consisting of one primary. The choice of $Si(OH)_4$ as the gas-phase monomer is motivated by the kinetic model developed in previous work [27] where $Si(OH)_4$ was deduced to be the main product of tetraethoxysilane decomposition. The formation of a single particle from gas-phase monomers ($Si(OH)_4$) is represented in **Fig. 3**.

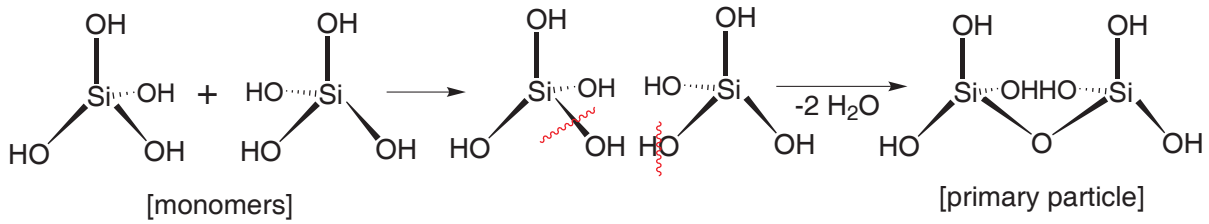


***Figure 3:*** *Inception of primary particles from gas-phase monomers.*

An inception event introduces a new particle into the system with initial composition as two Si units, one O unit and six OH units.

- **Surface Reaction:** A surface reaction is the reaction of a gas-phase monomer ($Si(OH)_4$) with an active site on a particle. The surface reaction between $Si(OH)_4$ and an –OH site on the particle is a dehydration reaction (removal of $H_2O$) and is represented in **Fig. 4**.

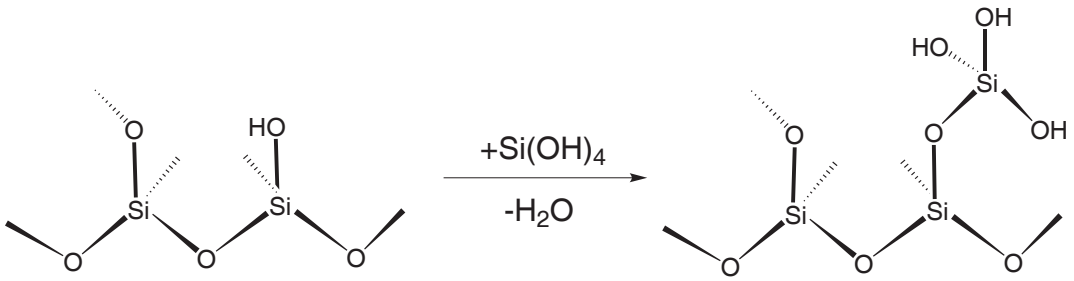


***Figure 4:*** *Surface reaction between a particle and a gas-phase molecule.*

The reaction of a gas-phase molecule on the particle surface alters its chemical composition. The composition of a randomly chosen primary particle is altered by increasing the chemical units of Si by one, O by one and OH by two.

***Surface Rounding:*** Surface reactions also alter the common surface of a primary with other primaries and thus bring about surface rounding as depicted in **Fig. 5**.

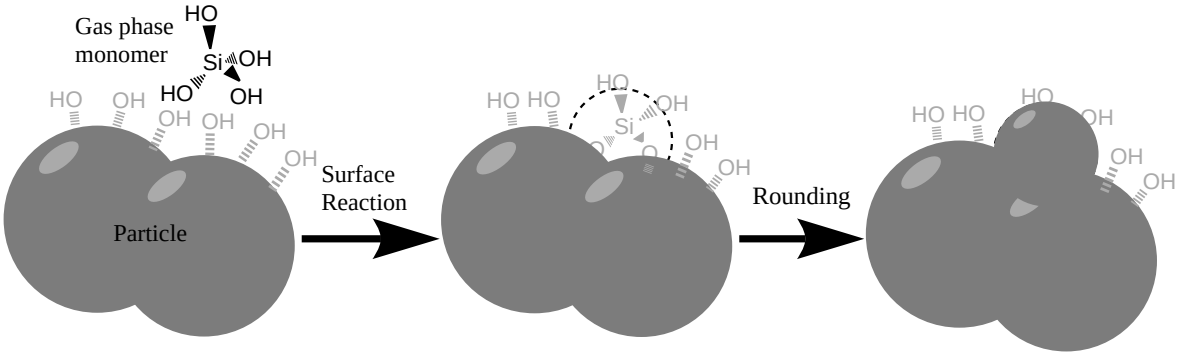


***Figure 5:*** *Surface rounding due to reaction of a gas-phase molecule on particle surface.*

The change in volume due to surface reaction, results in the change in net common surface area between the transformed primary particle and all of its neighbouring primaries. This net change in common surface area is calculated using:

$$\Delta s = \Delta v \frac{2\sigma}{d_{\mathrm{p}}}, \tag{1}$$

where $\Delta v$ is the change in volume brought about by surface reaction, $d_{\mathrm{p}}$ is the primary particle diameter of the transformed primary and $\sigma$ is the coalescence threshold for surface rounding ($0 \leq \sigma \leq 2$) [24], and is a free parameter in the current model.

- **Coagulation:** Coagulation occurs when two particles collide with each other and instantaneously stick together to form a new particle. Coagulation between two particles is represented in **Fig. 6**.

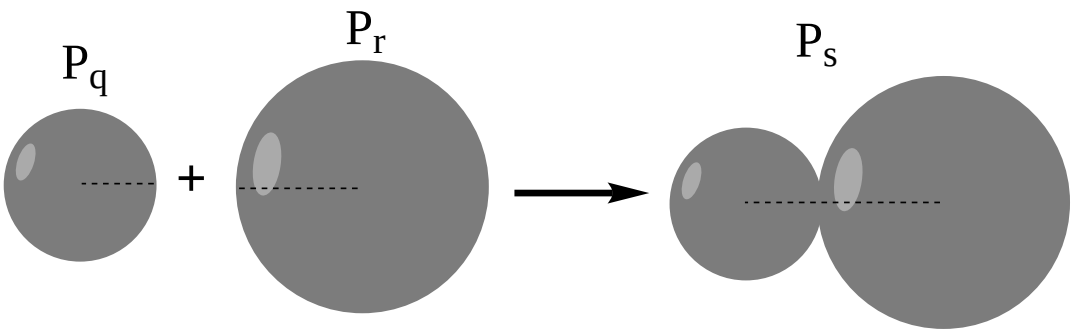


***Figure 6:*** *Coagulation between two particles.*

Coagulation of two particles forms a new particle such that the primaries of the two particles are the same as the primaries of the new particle. After coagulation, the two particles are assumed to be in point contact and the connectivity of the new particle is updated accordingly. The chemical composition of the particles remains invariant.

- **Sintering:** Sintering minimises the surface energy of a particle and therefore increases its sphericity. In this work, sintering between different primaries in a single particle is calculated on a localized level (primary-particle level) using the approach outlined by Sander et al. [23]. Sintering of silica nanoparticles is described by the viscous flow model [6]. The time evolution of the sintering process for a single particle is represented in **Fig. 7**

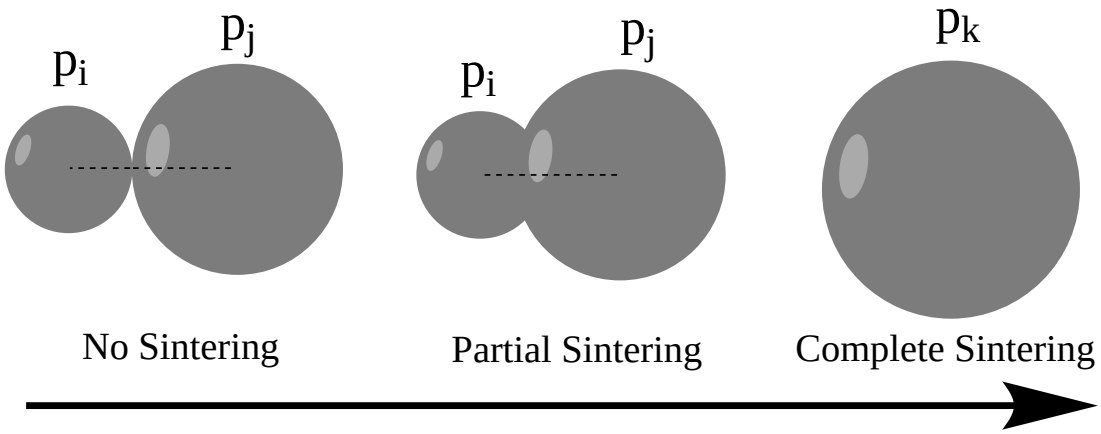


***Figure 7:*** *Evolution of sintering process with time.*

The degree of sintering between two primaries $p_i$ and $p_j$ is indicated by its sintering level defined as:

$$s(p_i, p_j) = \frac{\frac{S_{\text{sph}}(p_i,p_j)}{C_{ij}} - 2^{\frac{1}{3}}}{1 - 2^{\frac{1}{3}}}, \tag{2}$$

where $S_{\text{sph}}(p_i, p_j) = \sqrt[3]{\pi}(6(v(p_i) + v(p_j)))^{\frac{2}{3}}$ is the surface area of a sphere with the same volume as the two primaries.

The transformation of particle $P_q$ is conditional on the value of the sintering level $s(p_i, p_j)$. Two kinds of transformations are defined based upon a threshold value of sintering level at 95%. The primaries are assumed to be partially sintered if $s(p_i, p_j) < 0.95$ and are assumed to be fully sintered if $s(p_i, p_j) \geq 0.95$.

The –OH sites on surface of one primary react with the –OH sites on the surface of the second primary to form Si–O–Si bonds at the particle neck and release $H_2O$ molecules into the gas-phase. Thus, sintering also alters the composition of a particle as shown in **Fig. 8**.

- **Intra-particle reaction:** Intra-particle reaction is the reaction of two adjacent –OH sites on a single particle and results in the reduction of –OH units in the particle as depicted in **Fig. 9**. At steady state, the stoichiometric ratio of Si:O in a particle converges to a ratio of 1:2 and there are no –OH sites present on the particle surface.

Intra-particle reaction is modelled by changing the chemical composition of a randomly selected primary within a particle; the number of –OH sites is reduced by two and the number of O sites is increased by one.

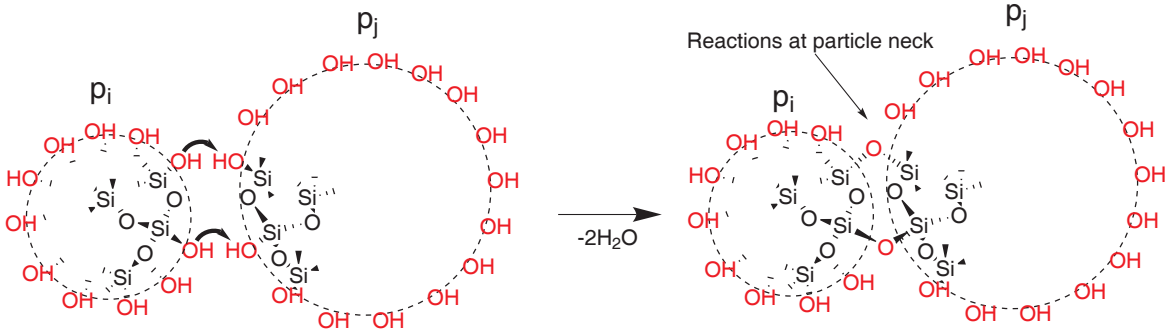


***Figure 8:*** *Dehydration reaction due to sintering.*

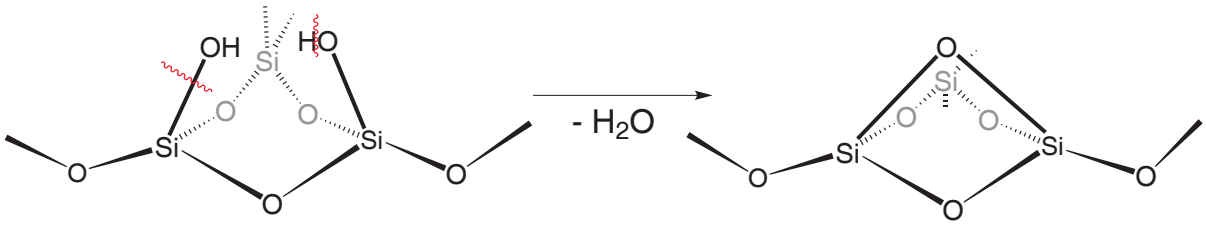


***Figure 9:*** *Intra-particle reaction.*

## 2.2 Rates of individual processes

- **Inception:** A new particle is inserted within the particle ensemble each time two molecules from the gas-phase collide. This rate is given by the rate of irreversible bimolecular reaction:

$$\mathrm{Si(OH)_4 + Si(OH)_4 \rightarrow Si(OH)_3\text{–}O\text{–}Si(OH)_3 + H_2O.} \tag{3}$$

The rate is calculated using the free molecular kernel:

$$R_{\mathrm{inc}} = \frac{1}{2} K^{\mathrm{fm}} {N_A}^2 C_{\mathrm{g}}^2, \tag{4}$$

where $N_{\mathrm{A}}$ is Avogadro's number, $C_{\mathrm{g}}$ is the gas-phase concentration of the incepting species and $K^{\mathrm{fm}}$ is the free molecular regime coagulation kernel given by:

$$K^{\mathrm{fm}} = 4\sqrt{\frac{\pi k_{\mathrm{B}} T}{m_{\mathrm{g}}}} d_{\mathrm{g}}^2, \tag{5}$$

where $k_{\mathrm{B}}$ is Boltzmann's constant, $T$ is the system temperature, $m_{\mathrm{g}}$ and $d_{\mathrm{g}}$ are the mass and diameter respectively of the gas-phase molecule $\mathrm{Si(OH)_4}$.

- **Surface Reaction:** A molecule from the gas-phase reacts with a particle and increases its mass. This process is implemented in the model by assuming that the collision of a molecule from the gas-phase and a particle can be calculated using

the free molecular collision kernel for the particle and a single molecule from the gas phase. Since the rate of reaction is the rate of *reactive* collisions, the rate takes the form:

$$R_{\text{surf}} = A_{\text{surf}} \exp\left(-\frac{E_{\text{a}}}{RT}\right) \eta_{\text{OH}} N_{\text{A}} C_{\text{g}}, \tag{6}$$

$A_{\text{surf}}$ is pre-exponential factor (obtained from collision theory), $E_{\text{a}}$ is activation energy, $\eta_{\text{OH}}$ is the total number of –OH sites on particle and $C_{\text{g}}$ is the gas-phase concentration of the reacting species. $A_{\text{surf}}$ has to be determined empirically or using theoretical calculations like plain-wave DFT methods. However, in the current model, $A_{\text{surf}}$ is set to the collision limit ($1 \times 10^{13}$), $E_{\text{a}}$ is the activation energy for a dehydration reaction between two –OH reactions (currently set to 0) and $T$ is the temperature.

- **Coagulation:** The coagulation rate between $P_q$ and $P_r$ is calculated using the transition coagulation kernel:

$$K^{\text{tr}} = \frac{K^{\text{sf}} K^{\text{fm}}}{K^{\text{sf}} + K^{\text{fm}}}, \tag{7}$$

where $K^{\text{sf}}$ is the slip-flow kernel and $K^{\text{fm}}$ is the free-molecular kernel.

- **Sintering:** The sintering rate $R_{\text{sint}}$ depends on the excess surface of the particle over a spherical particle with the same mass. A particle spontaneously reduces its free surface to minimise the free energy. This results in the rounding of the particle, finally to a sphere. The rate of sintering between two primaries is equivalent to the rate of change of their common surface $\Delta C_{ij}$ in time $\Delta t$:

$$\frac{\Delta C_{ij}}{\Delta t} = -\frac{1}{\tau(p_i, p_j)}(C_{ij} - S_{\text{sph}}(p_i, p_j)), \tag{8}$$

where $S_{\text{sph}}(p_i, p_j)$ is the surface area of a sphere with the same volume as the two primaries. $\tau(p_i, p_j)$ is the characteristic sintering rate calculated using the formula of Tsantilis et al. [35] as:

$$\tau(p_i, p_j) = A_{\text{s}} \times d_{\text{p}}(p_i, p_j) \times \exp\left(\frac{E_{\text{s}}}{T}\left(1 - \frac{d_{\text{p,crit}}}{d_{\text{p}}(p_i, p_j)}\right)\right), \tag{9}$$

where $d_{\text{p}}(p_i, p_j)$ is the minimum diameter of $p_i$ and $p_j$, and $A_{\text{s}}$, $E_{\text{s}}$ and $d_{\text{p,crit}}$ (the sintering parameters) are free parameters in this model.

- **Intra-particle reaction:** The rate of intra-particle reaction is deduced from the rate of surface reaction and the average sintering rate and is described in detail in the following section.

## 2.3 Stoichiometric ratio of Si:O

The interplay between the rates of different processes should be such that the stoichiometric ratio of Si:O is consistent with the experimentally observed ratio of 1:2. Using

this constraint, the rate of intra-particle reaction can be deduced. The chemical units in particle $P_q$ vary with time $t$. After a time interval of $\Delta t$, the following events occur which transform particle $P_q$ :

1. Let the average number of surface reaction events that occur in $\Delta t$ be $N_{\text{surf}}(P_q)$.
2. Let the average number of intra-particle events that occur in $\Delta t$ be $N_{\text{int}}(P_q)$.
3. Let the average number of OH units that are reduced by sintering in time $\Delta t$ be $\Delta_{\text{sint}}\eta_{\text{OH}}(P_q)$.

Using the jumps associated with each of these processes defined in §2.1, we find the changes in Si, O and OH units of particle $P_q$ to be:

$$\Delta\eta_{\text{Si}}(P_q) = N_{\text{surf}},$$

$$\Delta\eta_{\text{O}}(P_q) = N_{\text{surf}} + N_{\text{int}} + \frac{\Delta_{\text{sint}}\eta_{\text{OH}}(P_q)}{2},$$

$$\Delta\eta_{\text{OH}}(P_q) = 2N_{\text{surf}} - 2N_{\text{int}} - \Delta_{\text{sint}}\eta_{\text{OH}}(P_q).$$

The total change in O units of the particle is given by the sum of the changes in free O units ($\Delta\eta_{\text{O}}(P_q)$) and OH units ($\Delta\eta_{\text{OH}}(P_q)$). Thus, $\Delta\eta_{\text{O,total}}(P_q) = \Delta\eta_{\text{O}}(P_q) + \Delta\eta_{\text{OH}}(P_q)$. The ratio of Si to O is thus given by:

$$\frac{\Delta\eta_{\text{Si}}(P_q)}{\Delta\eta_{\text{O,total}}(P_q)} = \frac{N_{\text{surf}}}{3N_{\text{surf}} - N_{\text{int}} - \frac{\Delta_{\text{sint}}\eta_{\text{OH}}(P_q)}{2}}. \tag{10}$$

The stoichiometric ratio of Si:O in particle $P_q$ has to be 1:2 in order to be consistent with experimental observations. By assuming that the number of events of each process are much greater than the initial number of Si, O and OH in $P_q$, substituting in Eq. 10 we get,

$$\frac{N_{\text{surf}}}{3N_{\text{surf}} - N_{\text{int}} - \frac{\Delta_{\text{sint}}\eta_{\text{OH}}(P_q)}{2}} := \frac{1}{2} \tag{11}$$

$$\implies N_{\text{int}} = N_{\text{surf}} - \frac{\Delta_{\text{sint}}\eta_{\text{OH}}(P_q)}{2}. \tag{12}$$

Dividing Eq. 12 by $\Delta t$, we get:

$$R_{\text{int}} = R_{\text{surf}} - \frac{\Delta_{\text{sint}}\eta_{\text{OH}}(P_q)}{2\Delta t}. \tag{13}$$

The surface density of OH sites is assumed to be constant throughout the sintering process. The reduction in surface area due to sintering is thus accompanied by a reduction in the

number of OH sites. The change in the number of OH in particle $P_q$ due to sintering is given by:

$$\frac{\Delta_{\text{sint}}\eta_{\text{OH}}(P_q)}{2\Delta t} = \frac{\rho_{\text{s}}(P_q)}{2}\frac{\Delta S(P_q)}{\Delta t}, \tag{14}$$

where $\Delta S(P_q)$ is the net change in surface of $P_q$ due to sintering and $\rho_{\text{s}}(P_q) = \eta_{\text{OH}}(P_q)/S(P_q)$ is the surface density of OH sites. Since the change in surface area of $P_q$ is the sum of the change of surface areas of all its constituent primaries, we get:

$$\frac{\Delta S(P_q)}{\Delta t} = \sum_{i,j=1}^{n(P_q)} \frac{\Delta C_{ij}}{\Delta t}. \tag{15}$$

Substituting the value of the rate of change of surface ($\Delta C_{ij}/\Delta t$) from Eq. 8, we get the overall rate of intra-particle reaction for particle $P_q$:

$$R_{\text{int}}(P_q) = A_{\text{surf}} \exp\left(-\frac{E_{\text{a}}}{RT}\right)\eta_{\text{OH}}(P_q)N_{\text{A}}C_{\text{g}} - \frac{\rho_{\text{s}}(P_q)}{2}\left[\sum_{i,j=1}^{n(P_q)} \frac{C_{ij} - S_{\text{sph}}(p_i, p_j)}{\tau(p_i, p_j)}\right]. \tag{16}$$

The silica particle model described above is solved using a stochastic particle algorithm and linear process deferment algorithm [20]. The particle model is two-way coupled to the gas-phase kinetic model of Shekar et al. [27] using an operator splitting technique [2, 3].

# 3 Parameter estimation

The accurate estimation of model parameters is crucial to the performance of the model [14]. In this section, the free parameters in the model are determined by fitting the model to the experimental conditions of Seto et al. [26] who evaluate the sintering characteristics of silica nanoparticles by observing the change in size and size distribution of nanoparticle agglomerate in a heated pipe. The nanoparticles, initially formed at 900 °C, are heated to six different final temperatures and their collision and primary particle diameters observed.

The silica particle model described in §2 has four free-parameters:

1. $A_{\text{s}}$ : Pre-exponential factor for sintering (§2.2)
2. $E_{\text{s}}$ : Activation energy of sintering (§2.2)
3. $d_{\text{p,crit}}$ : Critical diameter below which the particles are considered to be liquid-like and sinter instantaneously (§2.2)
4. $\sigma$ : Coalescence threshold for surface rounding (§2.1).

The parameter space in the current model is thus four-dimensional and is given by:

$$\boldsymbol{y} = (A_\mathrm{s}, E_\mathrm{s}, d_\mathrm{p,crit}, \sigma). \tag{17}$$

The initial values of the sintering parameters ($A_\mathrm{s}$, $E_\mathrm{s}$ and $d_\mathrm{p,crit}$) were taken from a previous work [27] and the initial value of the coalescence threshold was set to 1.

A two-step optimisation method similar to that used by Brownbridge et al. [1] to automate IC engine model development is implemented to estimate the parameter values:

1. Data points in the four-dimensional space are generated using quasi-random low discrepancy Sobol sequences [31]. The model is evaluated at these points and the objective function $\Phi(\boldsymbol{y})$ determined as:

$$\Phi(\boldsymbol{y}) = \sum_{i=1}^{N_\mathrm{exp}} \left( [\langle d_{\mathrm{c}_i}^\mathrm{exp} \rangle - \langle d_{\mathrm{c}_i}^\mathrm{sim} \rangle(\boldsymbol{y})]^2 + [\langle d_{\mathrm{p}_i}^\mathrm{exp} \rangle - \langle d_{\mathrm{p}_i}^\mathrm{sim} \rangle(\boldsymbol{y})]^2 \right), \tag{18}$$

   where $N_\mathrm{exp}$ is the number of experimental points from Seto et al. [26]. $d_{\mathrm{c}_i}^\mathrm{exp}$, $d_{\mathrm{p}_i}^\mathrm{exp}$, $d_{\mathrm{c}_i}^\mathrm{sim}$ and $d_{\mathrm{p}_i}^\mathrm{sim}$ are the experimental and simulated collision and primary particle diameters respectively. The set of parameters that minimises the objective function $\Phi(\boldsymbol{y})$ is first determined.

2. For the next step of parameter estimation, the model is optimised using the simultaneous perturbation stochastic approximation (SPSA) algorithm [32]. SPSA is a descent method where the gradient is approximated using two measurements of the objective function. A new set of parameters that further minimises Eq. 18 is determined.

The resulting parameter values estimated using Sobol sequences followed by an SPSA algorithm are shown in **Table 1**.

***Table 1:*** *Values of sintering parameters in the particle model compared to values calculated by Shekar et al. [27].*

| Parameter | Value [27] | Value (current model) |
|---|---|---|
| $A_\mathrm{s}$ ($\mathrm{m}^{-1}\mathrm{s}$) | $1.16 \times 10^{-16}$ | $3.49 \times 10^{-14}$ |
| $E_\mathrm{s}$ (K) | $12.7 \times 10^{4}$ | $11.44 \times 10^{4}$ |
| $d_\mathrm{p,crit}$ (m) | $4.4 \times 10^{-9}$ | $5.76 \times 10^{-9}$ |
| $\sigma$ (-) | 0 | 1.972 |

The optimised model response, *i.e.* , the average collision diameter and particle diameter at different final temperatures is shown in **Fig. 10**

To establish the consistency of the model with experiments, other model results are compared to experimental observations. **Figs. 11a, 11b and 11c** compare the particle size distributions (PSDs) with respect to primary particle diameter ($d_\mathrm{p}$) and collision diameter ($d_\mathrm{c}$) obtained from simulation and experiments at three different final temperatures.

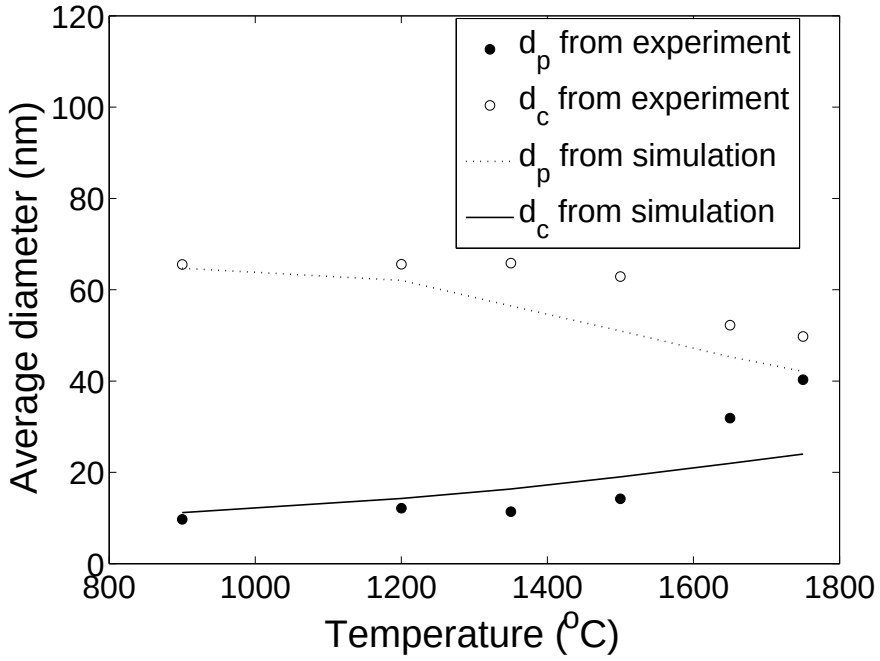


***Figure 10:*** *Optimised model response,* i.e. *average primary diameter ($d_p$) and collision diameter ($d_c$) at different final temperatures.* $^{(a)}$*Experimental values are from Seto et al. [26].*

Also presented are the corresponding TEM images generated by projecting the particles on to an $x - y$ plane to simulate the transmission of an electron beam through a particle specimen.

In Fig. 11a, at 900 °C, the primary particle size distribution is narrow with a low mean as the primaries are not sintered and hence are of uniform size. The corresponding collision diameter PSD is broad with higher mean due to high degree of agglomeration and low levels of sintering. The inlaid TEM image confirms the observations from the PSD where high agglomeration and low sintering is observed. As the final temperature is increased to 1500 °C (Fig. 11b), the primary diameter PSD gets broader and the collision diameter gets narrower due to sintering. The corresponding TEM image reflects this observation, the collision diameter of particles decreases while the corresponding mean primary diameter increases. In Fig. 11c at 1750 °C, the particles are highly sintered. The size distributions of primary and collision diameters are close to each other because the particles sinter completely increasing the size of the primaries and reducing the size of the particles. The corresponding TEM image shows particles that are small in size and almost spherical in shape. These simulation results are found to be in close agreement with the experimental observations.

# 4 Simulation Results and Discussion

The sensitive applications of silica nanoparticles require effective control of particle properties. The product applications depend on particle size distribution, morphology, degree

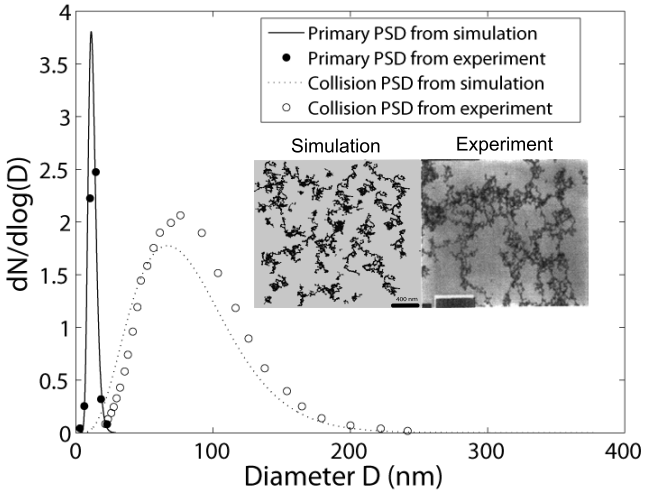


**(a)** $\mathrm{T} = 900\,^{\circ}\mathrm{C}$

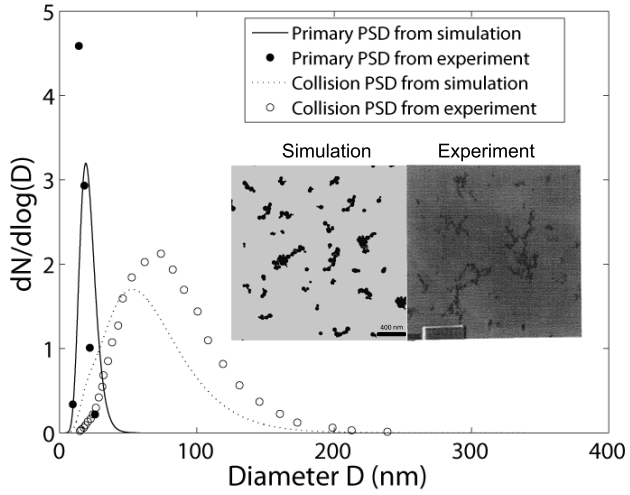


**(b)** $\mathrm{T} = 1500\,^{\circ}\mathrm{C}$

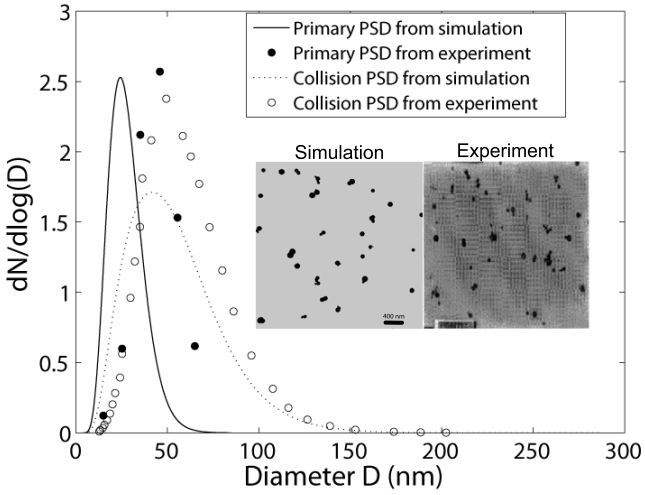


**(c)** $\mathrm{T} = 1750\,^{\circ}\mathrm{C}$

***Figure 11:*** *Particle size distribution and corresponding TEMs at different final temperatures. The experimental data are from Seto et al. [26].*

of agglomeration in addition to surface chemistry. In the industrial production of SiNP, emphasis is laid on understanding how to attain product control by varying the process conditions. The characterisation of size, surface activity, and degree of agglomeration within the nanoparticles is also essential with a view to performing toxicological studies [12].

Having estimated the unknown parameters in §3, this section reports industrially relevant model results at different process conditions. The zones of operating conditions for desirable product properties have also been highlighted. In particular, the effects of varying the key process variables, namely, the reactor temperature and inlet concentration have been examined. The values of the key process variables are listed in **Table 2** [8, 33].

***Table 2:*** *Key process variables in an industrial flame reactor.*

| Parameter | Value |
|---|---|
| Temperature | $1000\ \text{K} \leq T \leq 2000\ \text{K}$ |
| Pressure | $P = 1$ atm |
| Residence time | $10\ \text{ms} \leq \tau_\text{r} \leq 100\ \text{ms}$ |
| Precursor mole-fraction | $100\ \text{ppm} \leq x_{0,\text{TEOS}} \leq 10,000\ \text{ppm}$ |

The results reported in this section have been produced by simulating an isothermal batch reactor at a range of reactor temperatures ($1200\ \text{K} \leq T_0 \leq 2000\ \text{K}$) and initial TEOS mole-fractions ($80\ \text{ppm} \leq x_{0,\text{TEOS}} \leq 8000\ \text{ppm}$).

## 4.1 TEOS decomposition rate

The rate of decomposition of TEOS is an essential parameter to determine the amount of gas-phase monomers in the system, and thus significantly effects the final particle properties. The precursor (TEOS) decomposition rate is highly sensitive to the key operating conditions such as temperature and initial concentration of species. The decomposition time for complete conversion of TEOS at different process conditions is shown in **Fig. 12**.

The decomposition time reduces with increasing temperature, *i.e.* , the rate of conversion is faster at higher temperatures as predicted by the Arrhenius rate law. The conversion time increases insignificantly with increasing initial TEOS concentration.

## 4.2 Particle size distributions

Particle size distributions provide the primary characterisation of nanoparticles, with many industrial applications requiring particles of highly specific sizes and a narrow size distribution. The effect of varying the process conditions on the mean collision diameter of particle is depicted in **Fig. 13**. The highlighted zone represents the process conditions for desirable industrial operations details of which will be discussed in §4.4. **Zone A** indicates the process conditions required for nanoparticle applications requiring mean particle diameter between 40-80 nm.

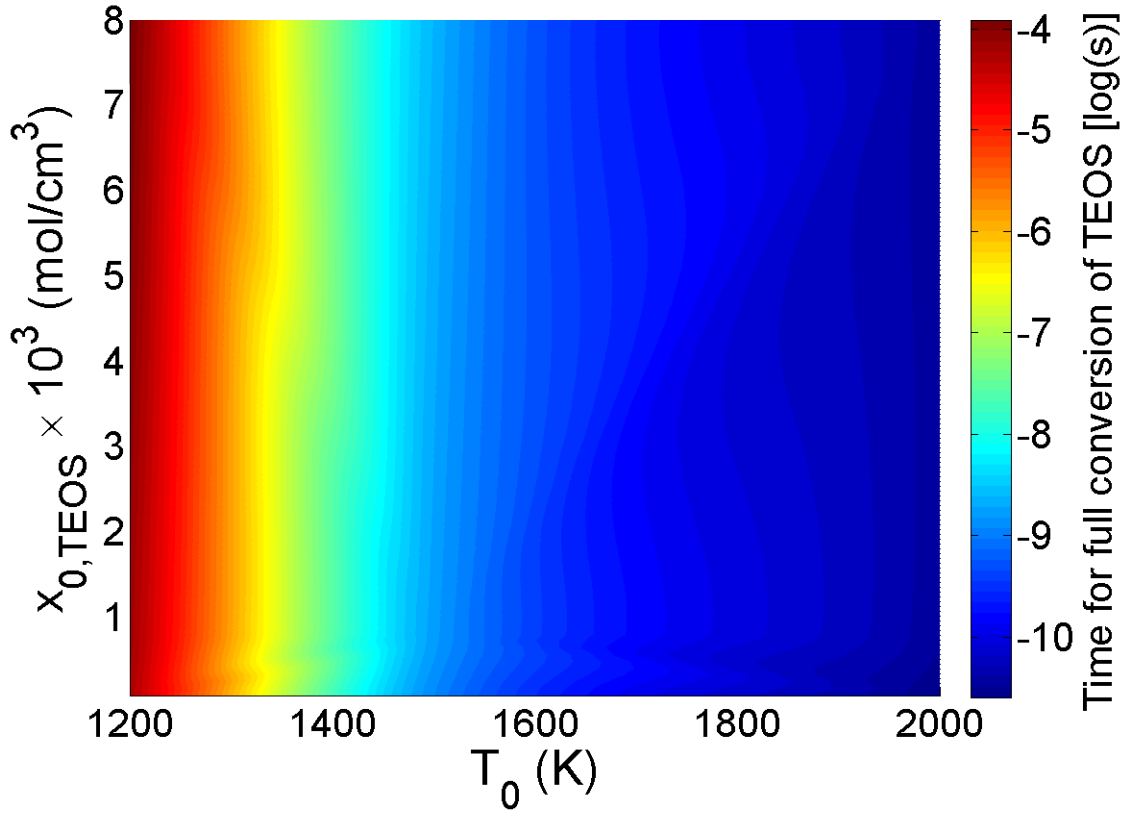


***Figure 12:*** *Effect of varying the process conditions on TEOS decomposition rate.*

At low temperatures, the mean collision diameter is small due to low conversion of TEOS to $Si(OH)_4$ (as depicted in Fig. 12). The low monomer ($Si(OH)_4$) concentration results in the formation of fewer particles resulting in negligible agglomeration. Thus, the particles are small in size and spherical in shape due to instantaneous sintering. As the temperature is increased, the conversion of TEOS to $Si(OH)_4$ increases resulting in more agglomerated particles with a greater mean collision diameter. At high temperatures, the particle size reduces due to the pronounced effect of sintering, which increases the sphericity of the particles and reduces the mean diameter.

The effect of the process conditions on the standard deviation of the collision diameter of a particle ensemble is shown in **Fig. 14**. Industrial applications typically favour particles with a narrow size distribution or a lower value of standard deviation ($\leq$ 25 nm) which are indicated as **Zone B** in Fig. 14.

The particle size distribution becomes wider with increasing values of $x_{0,\mathrm{TEOS}}$ due to an increase in the degree of agglomeration. The standard deviation is relatively small at low temperatures, due to low conversion of TEOS to $Si(OH)_4$ resulting in fewer particles present as incepted monomers. As the temperature is increased, the conversion increases but so does the sintering between particles. At medium temperature, the effect of agglomeration supersedes sintering, thus producing particles of varying sizes (high standard deviation). At high temperatures, sintering is predominant and particles are more uniform

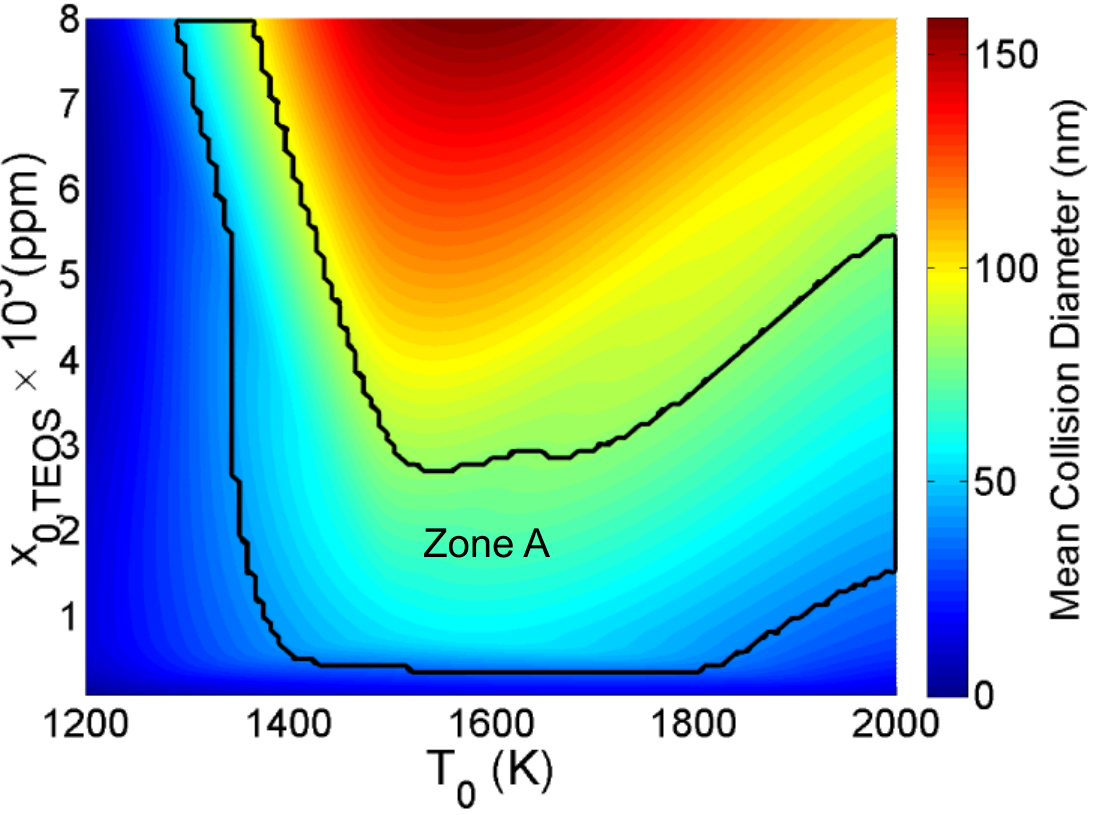


***Figure 13:*** *Effect of varying the process conditions on mean collision diameter. The highlighted zone indicates the desirable process conditions for industrial applications.*

in size and shape resulting in lower values of standard deviation.

## 4.3 Surface activity

The presence of hydroxyl groups on the silica nanoparticle surface has been reported in previous studies [40], which under suitable chemical treatment render many possibilities for surface functionalisation and thus can be effectively used for cellular drug delivery [17]. Radhakrishnan et al. [22] state that the hydroxyl groups on the surface of silica particles can easily be tailored with organic compounds or polymers to produce silica-polymer hybrid materials which are widely used as fillers in the manufacture of paints and rubber products. In light of these applications, surface characteristics of SiNP are an important property to track. The detailed particle description in the current model allows us to track the number of –OH sites per particle thus enabling a better understanding of surface activity. As depicted in **Fig. 15**, there is a direct positive correlation between the number of active sites and the temperature *i.e.* , as the temperature is increased the surface activity increases. As the TEOS concentration in the initial mixture is increased, the surface activity decreases. For an industrial application requiring high surface density of active sites, higher temperature operating conditions are preferred as highlighted by

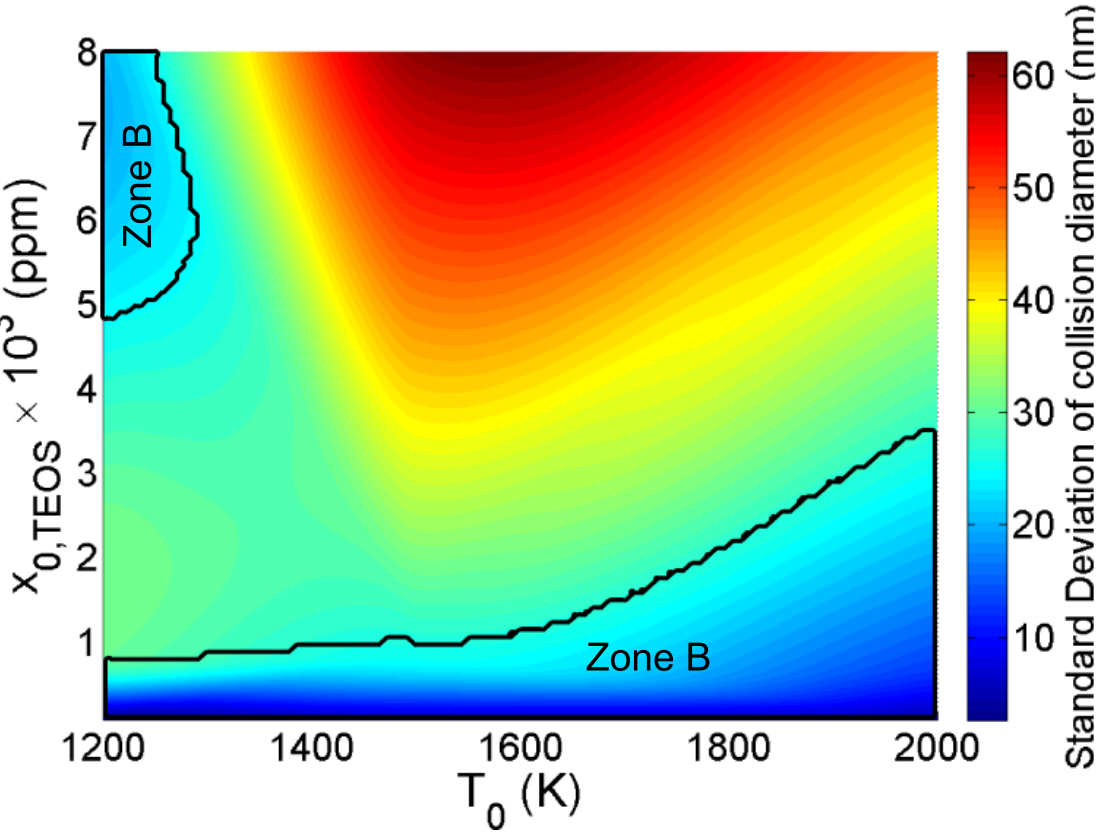


***Figure 14:*** *Effect of varying the process conditions on standard deviation of collision diameter distribution. The highlighted zones indicate the desirable process conditions for industrial applications.*

**Zone C** in Fig. 15.

## 4.4 Desirable process conditions for industrial applications

The various applications of silica nanoparticles in industries require the production of particles with highly specific properties. These desired properties vary amongst different applications. This section reports the process conditions that result in the production of silica nanoparticles suitable for key industrial applications.

**Functional material applications:** The use of SiNP as a funtional material for nanocomposites, electronics, optical and catalysis operation requires the mean particle size to be within a prescribed range, for example, between 40 nm and 80 nm and a narrow standard deviation (less than 25 nm) [15]. The desirable area of operation is the intersection of Zone A in Fig. 13 and Zone B in Fig. 14 and is shown in **Fig. 16**. The computer-generated TEM image of the ensemble at a characteristic operating condition is also depicted. It is observed that the particles are partially sintered at these conditions.

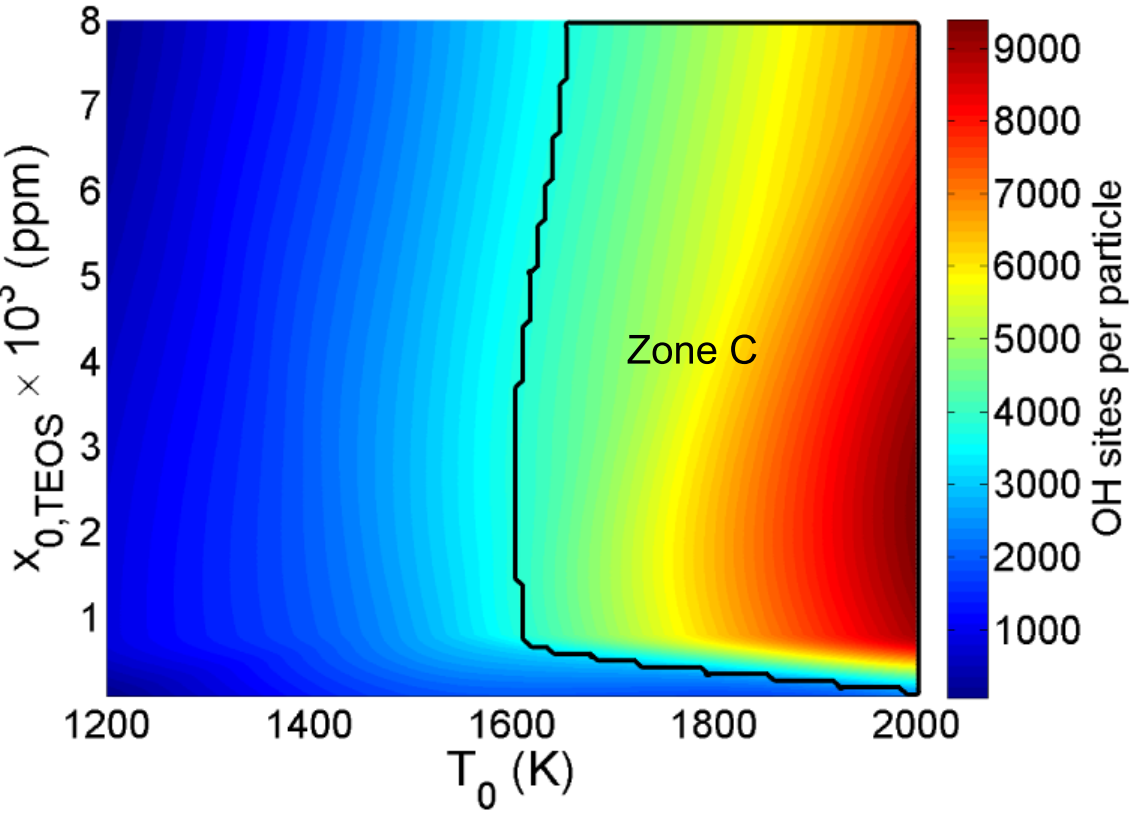


***Figure 15:*** *Effect of varying the process conditions on the number of OH sites per particle. The highlighted zone indicates the desirable process conditions for industrial applications.*

**Biomedical applications:** The application of silica nanoparticles in biotechnology is hypothesised to be derived from its active surface properties, *i.e.* , the presence of active –OH sites on the surface of the particle [40]. Thus, for biomedical applications, it is inferred that particles with a large number of active sites are desirable. Equally, for ease of cellular diffusion, particles of relatively small size and a narrow size distribution are required [29]. The desirable area of operation is the intersection of Zone A in Fig. 13, Zone B in Fig. 14 and Zone C in Fig. 15 as shown in **Fig. 17**. The computer-generated TEM image of the ensemble at a characteristic operating condition is also depicted. It is observed that the particles are closer to being fully sintered at these conditions.

**Evolution of particle morphology:** The size and morphology of silica nanoparticles greatly influence their physical and chemical properties, and determine their interaction with the environment and biological systems. Measuring size and morphology are therefore critically important to understanding the interactions between nanoscale materials and biological systems, as well as in understanding potential environmental risks. In **Fig. 18**, characteristic particles are overlayed onto the average sintering level contour plot at key process operating conditions to highlight the change in particle morphology and structure with respect to these operating conditions. At a low

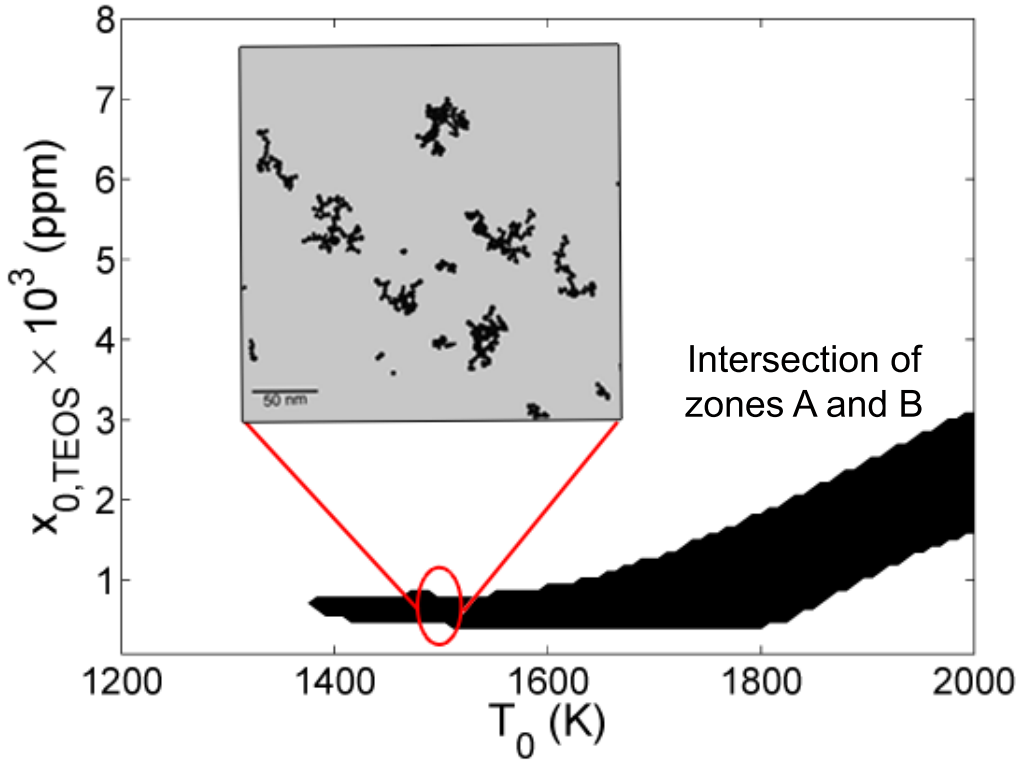


***Figure 16:*** *Desirable process conditions for functional material applications.*

temperature, the particles exist only as isolated primaries because there is limited conversion of the precursor (TEOS) to form gas-phase monomers ($Si(OH)_4$). As the temperature is increased from 1200 K to 1500 K, there is complete conversion of TEOS which results in the formation of bigger particles. On further increasing the temperature, the effect of sintering is dominant which makes the particles more spherical. These observations are consistent with the results of Zachariah et al. [41] and Schaefer and Hurd [25] indicating that temperature plays a significant role in the formation process, by controlling the chemical kinetic rates and through physical changes in particle morphology. It is also evident that increasing the initial precursor concentration results in the formation of more particles thereby increasing the aggregation of particles and reducing the average sintering level.

# 5 Conclusion

This work presents a new detailed multidimensional population balance model to describe the evolution of the chemical composition of silica nanoparticles formed from TEOS by aerosol synthesis. Each particle is represented in terms of its primary particles and the connectivity between these primaries. Each primary particle, in turn, is described by its chemical composition *i.e.* , the number of Si, O and OH groups present within it. Tracking the chemical composition of the particles allows us not only to describe the

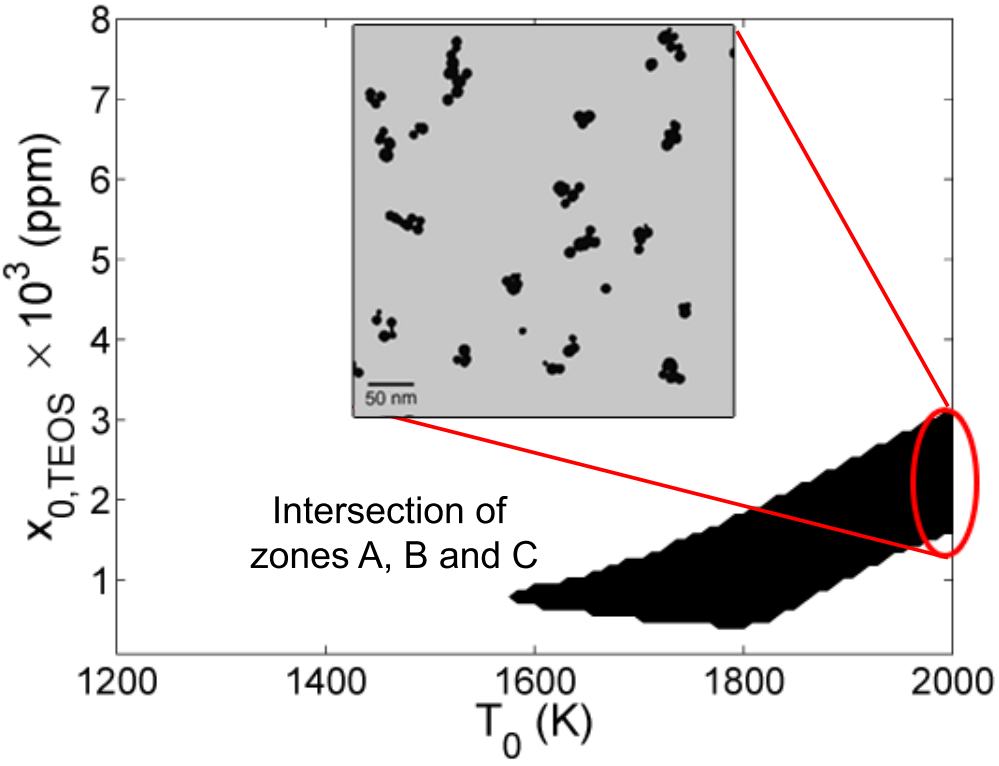


***Figure 17:*** *Desirable process conditions for biomedical applications.*

particle properties more accurately, but also provides better coupling of the gas-phase to the particle-phase.

Various particle processes have been included in the model that alter the state of the particle ensemble. In addition to nucleation, surface reaction, coagulation and sintering, the model also considers surface rounding and intra-particle processes. The rate of the intra-particle process is deduced by constraining the stoichiometric ratio of Si:O to 1:2. The rate of surface reaction is currently set to the collision limit, however quantum chemistry calculations may lead to more accurate rates for gas-surface interaction.

The free parameters in the model were estimated by fitting the model to experimental values of collision and primary particle diameters using Sobol sequences and the SPSA algorithm. The particle size distributions and computer-generated TEM images at different temperatures were compared with experimental observations and good agreement was found. Finally, an industrial isothermal batch reactor was simulated at different process conditions and various industrially important properties were reported. It was observed that as the process temperature increases, the average aggregate size reduces and the size distribution becomes narrower. The surface activity and average sintering level of particles also increase with increasing temperature. An increase in the inlet TEOS concentration increases the aggregate size, but reduces surface activity and average sintering level. An analysis of the process conditions required for a desirable range of particle properties was performed with a view to better industrial process control and optimisation. Future work would involve facilitating reactor design by interfacing the particle model with compu-

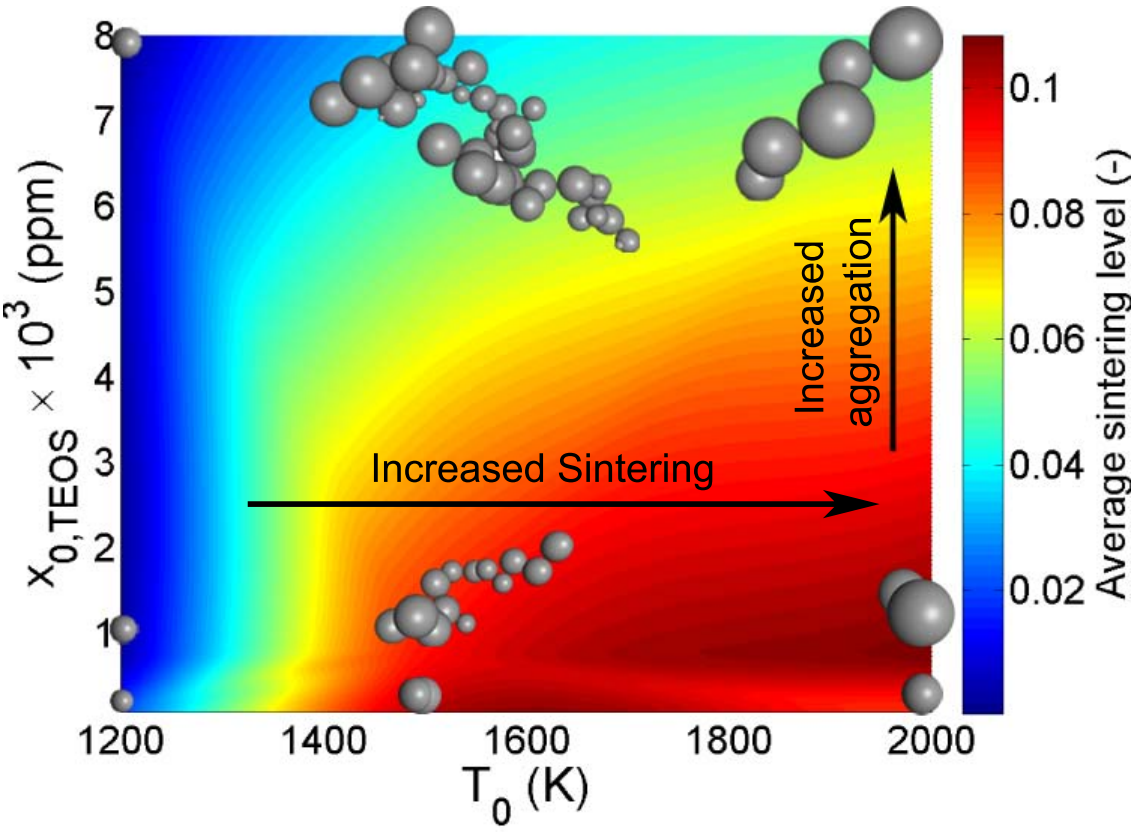


***Figure 18:*** *Average sintering level with respect to process conditions. Overlaid is the evolution of particle morphology.*

tational fluid dynamics (CFD). This work brings us closer to the overall goal of model development for engineering applications: to obtain more information about the system which are difficult to determine experimentally and to improve the accuracy of model prediction.

# 6 Acknowledgements

The authors acknowledge financial support provided by HeiQ materials. SS is thankful to the Cambridge Commonwealth Trust and Murray Edwards BP Centenary bursary for funding her PhD. MK is grateful for the support of the University of Duisburg-Essen. The authors also thank members of the Computational Modelling Group for their guidance and support.

# References


[1] G. Brownbridge, A. J. Smallbone, W. Phadungsukanan, S. Mosbach, M. Kraft, and B. Johansson. Automated IC engine model development with uncertainty propagation. *SAE Technical Paper*, 2011. doi:10.4271/2011-01-0237.

[2] M. S. Celnik. *On the numerical modelling of Soot and Carbon Nantube Formation*. PhD thesis, University of Cambridge, 2007.

[3] M. S. Celnik, R. I. A. Patterson, M. Kraft, and W. Wagner. Coupling a stochastic soot population balance to gas-phase chemistry using operator splitting. *Combustion and Flame*, 148(3):158–176, 2007. doi:10.1016/j.combustflame.2006.10.007.

[4] M. S. Celnik, R. I. A. Patterson, , M. Kraft, and W. Wagner. A predictor-corrector algorithm for the coupling of stiff odes to a particle population balance. *Journal of Computational Physics*, 228(8):2758–2769, 2009. doi:10.1016/j.jcp.2008.12.030.

[5] A. Eibeck and W. Wagner. An efficient stochastic algorithm for studying coagulation dynamics and gelation phenomena. *SIAM Journal on Scientific Computing*, 22(3): 802–821, 2000. doi:10.1137/S1064827599353488.

[6] J. Frenkel. Viscous flow of crystalline bodies under the action of surface tension. *Journal of Physics USSR*, 9(5):385–391, 1945.

[7] M. Goodson and M. Kraft. An efficient stochastic algorithm for simulating nano-particle dynamics. *Journal of Computational Physics*, 183:210–232, 2002. doi:10.1006/jcph.2002.7192.

[8] M. Height. Personal communication, HeiQ burner details, 2009.

[9] P. Ho and C. F. Melius. Theoretical Study of the Thermochemistry of Molecules in the Si-C-H-C System. *Journal of Physical Chemistry*, 99(7):2166–2176, 1995. doi:10.1021/j100007a056.

[10] R. K. Iler. *The Chemistry of Silica: Solubility, Polymerization, Colloid and Surface Properties and Biochemistry of Silica*. WILEY, Toronto, Canada, 1979. ISBN 978-0-471-02404-0.

[11] H. D. Jang. Generation of silica nanoparticles from tetraethylorthosilicate (TEOS) vapor in a diffusion flame. *Aerosol Science and Technology*, 30(5):477–488, 1999. doi:10.1080/027868299304516.

[12] J. Jiang, G. Oberdörster, and P. Biswas. Characterization of size, surface charge, and agglomeration state of nanoparticle dispersions for toxicological studies. *Journal of Nanoparticle Research*, 11(1):77–89, 2009. doi:10.1007/s11051-008-9446-4.

[13] H. K. Kammler, L. Mädler, and S. E. Pratsinis. Flame synthesis of nanoparticles. *Chemical Engineering and Technology*, 24(6):583–596, 2001. doi:10.1109/9.119632.

[14] M. Kraft and S. Mosbach. The future of computational modelling in reaction engineering. *Philosophical Transactions of The Royal Society*, 368(1):3633–3644, 2010. doi:10.1098/rsta.2010.0124.

[15] F. E. Kruis, H. Fissan, and A. Peledt. Synthesis of nanoparticles in the gas phase for electronic, optical and magnetic applications: A review. *Journal of aerosol science*, 29(5-6):511–535, 1998. doi:10.1016/S0021-8502(97)10032-5.

[16] B. W. Lee, J. I. Jeong, J. Y. Hwang, M. Choi, and S. H. Chung. Analysis of growth of non-spherical silica particles in a counterflow diffusion flame considering chemical reactions, coagulation and coalescence. *Journal of Aerosol Science*, 32(2):165–185, 2001. doi:10.1016/S0021-8502(00)00054-9.

[17] S. Legrand, A. Catheline, L. Kind, E. C. Constable, C. E. Housecroft, L. Landmann, P. Banse, U. Pielesa, and A. Wirth-Heller. Controlling silica nanoparticle properties for biomedical applications through surface modification. *New Journal of Chemistry*, 32(4):588–593, 2008. doi:10.1039/b718668a.

[18] N. Morgan, C. Wells, M. Kraft, and W. Wagner. Modelling nanoparticle dynamics: Coagulation, sintering, particle inception and surface growth. *Combustion Theory and Modelling*, 9(3):449–461, 2005. doi:10.1080/13647830500277183.

[19] R. I. A. Patterson and M. Kraft. Models for the aggregate structure of soot particles. *Combustion and Flame*, 151:160–172, 2007. doi:10.1016/j.combustflame.2007.04.012.

[20] R. I. A. Patterson, J. Singh, M. Balthasar, M. Kraft, and J. Norris. The Linear Process Deferment Algorithm: A new technique for solving population balance equations. *SIAM Journal on Scientific Computing*, (28):303–320, 2006. doi:10.1137/040618953.

[21] W. Phadungsukanan, S. Shekar, R. Shirley, M. Sander, R. H. West, and M. Kraft. First-principles thermochemistry for silicon species in the decomposition of tetraethoxysilane. *Journal of Physical Chemistry A*, 113:9041–9049, 2009. doi:10.1021/jp905494s.

[22] B. Radhakrishnan, R. Ranjan, and W. J. Brittain. Surface initiated polymerizations from silica nanoparticles. *Soft Matter*, 2(5):386–396, 2006. doi:10.1039/B516508C.

[23] M. Sander, R. H. West, M. S. Celnik, and M. Kraft. A detailed model for the sintering of polydispersed nanoparticle agglomerates. *Aerosol Science and Technology*, 43 (10):978–989, 2009. doi:10.1080/02786820903092416.

[24] M. Sander, R. I. A. Patterson, A. Braumann, A. Raj, and M. Kraft. Developing the pah-pp soot particle model using process informatics and uncertainty propagation. *Proceedings of the Combustion Institute*, 33:675683, 2011. doi:10.1016/j.proci.2010.06.156.

[25] D. W. Schaefer and A. J. Hurd. Growth and structure of combustion aerosols: fumed silica. *Aerosol Science and Technology*, 12(4):876–890, 1990. doi:10.1080/02786829008959400.

[26] T. Seto, A. Hirota, T. Fujimoto, M. Shimada, and K. Okuyama. Sintering of Polydisperse Nanometer-Sized Agglomerates. *Aerosol Science and Technology*, 27(3): 422–438, 1997. doi:10.1080/02786829708965482.

[27] S. Shekar, M. Sander, R. Shaw, A. J. Smith, A. Braumann, and M. Kraft. Flame synthesis of silica nanoparticles from tetraethoxysilane. Technical Report 86, c4e-Preprint Series, Cambridge, 2010. URL como.cheng.cam.ac.uk/preprints/c4e-Preprint-86.pdf. Submitted to *Chemical Engineering Science*.

[28] S. Shekar, A. J. Smith, M. Sander, M. Kraft, and W. Wagner. Stochastic numerics for the gas-phase synthesis of nanoparticles, 2011. URL como.cheng.cam.ac.uk/presentations/ss663-presentation-coventry-2011.pdf. Invited presentation by M. Kraft on Monte Carlo Methods, Warwick Mathematics Institute, UK.

[29] I. I. Slowing, B. G. Trewyn, S. Giri, and V. S.-Y. Lin. Mesoporous silica nanoparticles for drug delivery and biosensing applications. *Advanced Functional Materials*, 17:1225–1236, 2007. doi:10.1002/adfm.200601191.

[30] J. Smolík and P. Moravec. Gas phase synthesis of fine silica particles by oxidation of tetraethylorthosilicate vapour. *Journal of Material Science Letters*, 14(6):387–488, 1995. doi:10.1007/BF00274548.

[31] I. M. Sobol. On the distribution of points in a cube and approximate evaluation of integrals. *USSR Computational Mathematics and Mathematical Physics*, 7:86–112, 1967.

[32] J. C. Spall. Multivariate stochastic approximation using a simultaneous perturbation gradient approximation. *IEEE Transactions on Automatic Control*, 37(3):332–341, 1992. doi:10.1109/9.119632.

[33] W. J. Stark and S. E. Pratsinis. Aerosol flame reactors for manufacture of nanoparticles. *Powder Technology*, 126(2):103–108, 2002. doi:10.1016/S0032-5910(02)00077-3.

[34] M. T. Swihart. Vapor-phase synthesis of nanoparticles. *Current Opinion in Colloid & Interface Science*, 8(1):127–133, 2003. doi:10.1016/S1359-029403.00007-4.

[35] S. Tsantilis, H. Briesen, and S. E. Pratsinis. Sintering time for silica particle growth. *Aerosol Science and Technology*, 34(3):237–246, 2001. doi:10.1080/02786820119149.

[36] S. Tsantilis, H. K. Kammler, and S. E. Pratsinis. Population balance modeling of flame synthesis of titania nanoparticles. *Chemical Engineering Science*, 57(12): 2139–2156, 2002. doi:10.1016/S0009-2509(02)00107-0.

[37] G. D. Ulrich. Theory of particle formation and growth in oxide synthesis flames. *Combustion Science and Technology*, 4(1):47–57, 1971. doi:10.1080/00102207108952471.

[38] R. H. West, M. S. Celnik, O. R. Inderwildi, M. Kraft, G. J. O. Beran, and W. H. Green. Towards a comprehensive model of the synthesis of $TiO_2$ particles from $TiCl_4$. *Industrial and Engineering Chemistry Research*, 46(19):6147–6156, 2007. doi:10.1021/ie0706414.

[39] Y. Xiong, M. K. Akhtar, and S. E. Pratsinis. Formation of agglomerate particles by coagulation and sintering–part II: The evolution of themorphology of aerosol-made titania, silica and silica-doped titania powders. *Journal of Aerosol Science*, 24(3): 301–313, 1993. doi:10.1016/0021-8502(93)90004-S.

[40] Z. P. Xu, Q. H. Zeng, G. Q. Lu, and A. B. Yu. Inorganic nanoparticles as carriers for efficient cellular delivery. *Chemical Engineering Science*, 61(3):1027 – 1040, 2006. doi:10.1016/j.ces.2005.06.019.

[41] M. R. Zachariah, D. Chin, H. G. Semerjian, and J. Katz. Silica particle synthesis in a counterflow diffusion flame reactor. *Combustion and Flame*, 78(3-4):287–298, 1989. doi:10.1016/0010-2180(89)90018-7.

# Citation index